On the Usage of Low-Cost MEMS Sensors, Strapdown Inertial Navigation and Nonlinear Estimation Techniques in Dynamic Positioning

Robert H. Rogne, Torleiv H. Bryne, Thor. I. Fossen and Tor A. Johansen

***Abstract*—In this article we suggest that a strapdown inertial navigation system based on MEMS inertial sensors is a useful addition to a vessel with dynamic positioning. We conduct full-scale experiments with MEMS inertial sensors on board a Dynamically Positioned (DP) offshore vessel operating off the Norwegian coast. The vessel operates in different scenarios, and the purpose is to showcase how low-cost MEMS sensors may complement or replace existing DP sensor systems. Employing nonlinear observers for estimating attitude, heave, velocity and position, we go through the benefits and disadvantages, and some caveats, for the sensors and methods used in this article. Two different MEMS units are evaluated, aided by gyrocompasses and position reference systems. We evaluate the attitude, heave and dead reckoning capabilities obtained with the presented estimators, in relation to relevant class notation, ultimately motivating the inclusion of new sensors and methods for dynamic positioning. The results related to attitude and heave are compared with data from well-proven industry standard vertical reference units while dead reckoning is evaluated with respect to the onboard position reference systems.**

***Index Terms*—Nonlinear Observers, Navigation, IMU, MEMS, Dynamic Positioning**

I. Introduction

Inertial sensors have been vital in the development of automatic control of ships since the first operational gyrocompasses were introduced prior to World War I. These gyrocompasses based on gimbal inertial sensor technology and physical self-alignment has been established as the main source of heading information on ships and free floaters. Other types of gyrocompasses also exist, the primary ones being Fiber Optic Gyroscopes (FOG), Hemispherical Resonant Gyroscopes (HRG) and Ring Laser Gyroscopes (RLG), [1].

Position Reference (PosRef) systems were introduced in more recent times, and include radio, laser, taut wire, hydroacoustic and satellite-based systems. The latter type has the benefit of world-wide coverage, and these systems are known collectively as Global Navigation Satellite Systems (GNSS), the most famous of which is the Global Positioning System (GPS).

In addition, so-called Vertical Reference Units (VRUs) are commonplace on a variety of vessels [2]. While gyrocompasses provide heading, VRUs complements them by providing the roll and pitch signals of a ship's motion. In some use cases the vessel's heave motion is also provided by this sensor. The roll and pitch estimates from VRUs are typically applied in lever arm compensation of position reference system measurements [3]. Other usages where the roll and pitch of a ship are of interest might include for instance ballasting systems. Heave estimates are of interest in heave compensation of cranes or drill floors during marine operation in waves, in heave displacement control of high-speed surface effect ships and for onboard decision support systems for e.g. weather prediction and sea state estimation.

For the usage of these types of sensors and systems in Dynamic Positioning (DP) vessels, the International Maritime Organization (IMO) has issued guidelines to reduce the risk of position-loss [4]. Maritime classification societies, such as DNV GL, American Bureau of Shipping (ABS), and Lloyd's Register (LR), have defined vessel class notations ranging from 1 to 3 based on the guidelines from IMO, where the class number depends on type of vessel and operation, and the potential consequences if loss of position occurs.

Generally in the class notations, a single fault must not lead to loss of position. To adhere to this fundamental rule, redundancy in all active components is usually required, where *redundancy* is defined by [5] as:

> *Redundancy*. The ability of a component or system to maintain its function when one failure has occurred. Redundancy can be achieved, for instance, by installation of multiple components, systems or alternative means of performing a function.

Specifically for class 2 and 3, MSC/Circ. 645 [4] states:

- Equipment class 2: Redundancy in all active components.
- Equipment class 3: Redundancy in all active components and physical separation (A.60) of a set of components.

where A.60 refers to a specific fire protection requirement. Class 1 allows for a single failure to lead to a loss of position, and will consequently not be dealt with further in this article. Table I describes in short the requirements for equipment class 2 and 3, and their equivalents by DNV GL, ABS and LR.

With regards to sensor systems, the demands stated by the equipment classes is typically implemented by just installing

The work has been carried out at the Centre for Autonomous Marine Operations and Systems (NTNU–AMOS) and supported by the Research Council of Norway and Rolls-Royce Marine (now Kongsberg Maritime CM) through the Centres of Excellence funding scheme and the MAROFF programme, grant numbers, 223254 and 225259 respectively. The Research Council of Norway is acknowledged as the main sponsor of NTNU–AMOS.

Robert H. Rogne, Torleiv H. Bryne, Thor I. Fossen and Tor A. Johansen are with the Centre for Autonomous Marine Operations, Department of Engineering Cybernetics, Norwegian University of Science and Techology, Trondheim 7491, Norway (e-mail: robert.rogne@ntnu.no, torleiv.h.bryne@ieee.org, fossen@ieee.org, tor.arne.johansen@ntnu.no).

TABLE I
DP CLASSIFICATIONS

Description	**IMO**	**Class notations**		
Demands related to position and heading control:	**DP Class**	**DNV GL**	**ABS**	**LR**
Single fault excluding loss of a compartment. Two independent computer systems. Specified maximum environmental conditions.	Class 2	DPS 2 DYNPOS-AUTR	DPS-2	DP (AA)
Single fault including loss of a compartment due to fire or flood. Two (or more) independent computer systems. Extra back-up system separated by A.60 class division). Specified maximum environmental conditions.	Class 3	DPS 3 DYNPOS–AUTRO	DPS-3	DP (AAA)

three of everything. In the authors' opinion, this strategy does not fully exploit the advantages of inertial sensors, and specifically not the recent developments of Micro-Electro-Mechanical System Inertial Measurement Units, or MEMS IMUs, and the awareness of the pros and cons of the typical vessel sensors and position reference systems. For instance, in the case of position reference systems, having three completely independent systems may be hard to achieve, as often only one or two independent systems are available at a given time. Installing three GNSS receivers and antennas will protect you from electronic failure of the components, but you are still vulnerable to external common mode failures related to satellite coverage. Chen et al. [6], investigates five different critical incidents from the North Sea where differential GNSS errors resulted in a drive-off or loss of position.

Bryne et al. [7] proposed an alternative sensor configuration for DP, using MEMS IMUs and appropriate software to

- provide an independent measurement principle for heading and position fault management,
- remove the need for dedicated VRUs,

all while potentially reducing the cost of DP sensor systems without compromising safety. In this article some of these principles are put to the test in a full-scale experiment to see if these claims have merit.

A. More on sensors and systems

In current vessels, MEMS inertial sensors together with an embedded computer and software are the foundation of the aforementioned VRUs [8].

In contrast to the gyrocompass and VRU, a full Inertial Navigation System (INS) applies tri-axial accelerometer and angular rate measurements to estimate three-degree-of-freedom Position, Velocity and Attitude (PVA) in a *dead reckoning* fashion. This entails that PVA is estimated relative some departure point by keeping track of the trajectory traveled. This is carried out by mechanization of the angular rate measurements and accelerometer measurements through the strapdown equations, (2), (6) and (7). Because of errors in the inertial sensor, such as noise and biases, dead reckoning is insufficient to maintain accurate estimates over time. To prevent the INS from drifting, aiding by position reference systems is often necessary, and an aided INS is often referred to as an integrated INS.

PosRefs are exposed to both natural degradation and deliberate outages. Natural degradation can be caused by signal distortion from reflection of nearby objects, known as multipath, loss of signal due to sun storms or loss of line of sight to the satellite. Deliberate outages can be because of signal jamming. During loss of PosRef, good dead reckoning capabilities are vital for the INS to provide accurate PVA estimates to the user, or to enable the INS' abilities to detect errors in the aiding sensors. As stated, DP classes require up to three independent PosRefs for safety reasons, but complete independence could be hard to achieve. In these cases, INS can serve as a technically independent system, providing position information through the integration of accelerometer data. Methods for combining INS and GNSS in a traditional way may be found in [9]–[11].

B. Nonlinear Estimation

The improvement of cost-effective MEMS IMUs over the last three decades has spurred the research on attitude estimation in general using NonLinear Observer (NLO) theory, such as [12]–[18]. The NLO of [16], based on [14], has been extended to make use of the translational motion obtained in a PosRef aided INS to improve the attitude observer's estimates, based on the theory of [19]. Examples of such results are [20], [21] where a three-degree-of-freedom position measurement is assumed available. Furthermore, [22]–[24] have tailored the result of [20] for marine surface navigation by replacing the need for a vertical PosRef measurement as navigation aid, with a Virtual Vertical Reference (VVR) measurement. In [25], the attitude observers of [26] and [20] were compared with regards to fault tolerance of heading and position reference errors.

The type of NLOs employed in this article have, unlike the Extended Kalman Filter (EKF), proven semiglobal exponential stability [20], [22]. Consequentially, we have some guarantees for robustness and convergence regardless of initialization. Additionally, since we do not need to propagate any Riccati equations as for the EKF, NLOs have the potential for being less of a computational burden.

Examples of heave estimation based on MEMS inertial sensors, using both linear and nonlinear methods, are presented in [22], [23], [27]–[29]. [27] and [29] are based on linear bandpass filtering, while [22], [23] is applying NLOs to estimate heave. In [24], a more sophisticated method evolving from [22], [23] is used, estimating wave motion parameters and employing these in the estimator.

C. INS in dynamic positioning

Considering ships with DP systems, the idea of fully integrated INSs is far from novel, as proposed in an industrial context almost 20 years ago [30], and later [31]. Up to present time such solutions have applied high-end IMUs, with FOG- or RLG-based angular rate sensors. The main aspiration of these products has been to filter PosRefs before applying them in the DP system. Also, [32] proposed that INS should be put in tandem with an acoustic system to detect anomalies in the GNSS and improve the performance of the DP system. However, many of the high-end integrated INS products for DP are subjected to strict export restrictions, limiting the market potential and increasing the cost of installation due to a possibly lengthy approval process before installation. MEMS-based IMUs are significantly less expensive and rarely subjected to export restrictions, which in it self motivates the investigation of applying these at the core of the onboard INS. This could also pave the way for cost-effective MEMS-based INS on a variety of ships from fishing vessels to bulk carriers and tankers.

TABLE II
CURRENT NUMBER OF SENSORS REQUIRED FOR DP BY DNV GL [5] (SIMPLIFIED)

Sensors		DPS 2	DPS 3
PosRef		3	2+1
External sensors	Wind	2	1+1
	Gyro compass	3	2+1
	VRS/VRU	2	2+1

+1 indicates A.60 fire proof physical separation of sensors.

TABLE III
ALTERNATIVE NUMBER OF SENSORS REQUIRED FOR DP INCORPORATING MEMS IMUS [7]

Sensors	Class 2	Class 3
PosRef	2	1+1
Gyro compass	2	1+1
MEMS IMU	3	3+3
Wind	(1)	(1)

+x indicates A.60 fire proof physical separation of sensors.

D. IMUs for improving DP classes

Table II presents the current DP sensor classifications by DNV GL [5], based on the guidelines put forward by the IMO [4]. These provide intuitive and straightforward triple redundancy, where one faulty sensor can be outvoted by the remaining ones. However, as pointed out in [7], this is not optimal as the gyros and accelerometers of the vertical reference systems are not typically integrated directly with the rest of the system, and thus cannot be used for fault detection in position reference systems or gyrocompasses. Table III presents an alternative sensor configuration, where the IMUs are used in a more unified manner. This way, the IMUs may be used in a fault detection framework based on redundant estimators. Three IMUs each consisting of an accelerometer- and a gyro-triad can themselves be made into a fairly reliable source for motion data [33]. Also, the VRU solution follows inherently from these sensors, which we will se later.

In the configuration in Tab. III the wind sensors are also optional, as the IMUs can measure the forces exerted on a vessel directly, as opposed to wind sensors which may provide data that is detrimental for usage in dynamic positioning [34].

As an alternative to reducing the number of sensors as in Tab. III, one could imagine still using the classic approach of Tab. II while including integrated MEMS IMUs. In this way, one may improve the redundancy and uptime of the DP system in the case of sensor failures, at a comparatively low upgrade cost. A DP operation would continue unhindered until a replacement sensor could be installed.

E. Main Contribution

The main contributions of this article comprise applying low-cost MEMS IMUs in the navigation system of a DP vessel, full-scale verification of different nonlinear observers for attitude estimation for ships, and showing how the IMUs may be a useful addition to or take the place of existing sensor systems, while maintaining safety in the context of DP class notations. We choose to use nonlinear observers in this article because of their proven stability properties, simplicity and intuitive structure. However, any method for position, velocity and attitude estimation could be employed in this context, where the most obvious alternative is the EKF.

The obtained results are compared to those of well-proven industrial sensor systems providing roll, pitch and heave measurements for marine surface vessels. Furthermore, to evaluate the aggregate performance of the navigation solution (combination of sensor quality and algorithm) we perform a dead reckoning test. The evaluation consist of:

- Applying two nonlinear observers — [14] and [23] — for ship attitude estimation.
- Applying the nonlinear observers and IMUs during two operation conditions: DP and turning maneuvers.
- Evaluation of heave estimation performance using a Virtual Vertical Reference (VVR) signal, [22], [23].
- Testing the potential of the underlying fault-tolerance properties of the integrated INS solutions by evaluating the dead reckoning capabilities of the IMU-and-estimator combinations.

Parts of this article are based on the preliminary work found in [35] and [36]. The work has been expanded with slightly better tuning to reflect the performance achievable with NLOs, low-pass filtering of IMU signals, comparison with EKF, and applying the VVR to a new observer. In addition, we discuss the philosophy of [7] and explore its plausibility with experimental data.

II. PRELIMINARIES

A. Notation

$\|\cdot\|_2$	the Euclidean vector norm
$\boldsymbol{I}_n$	$n \times n$ identity matrix
$(\cdot)^\intercal$	the transpose of a vector or a matrix

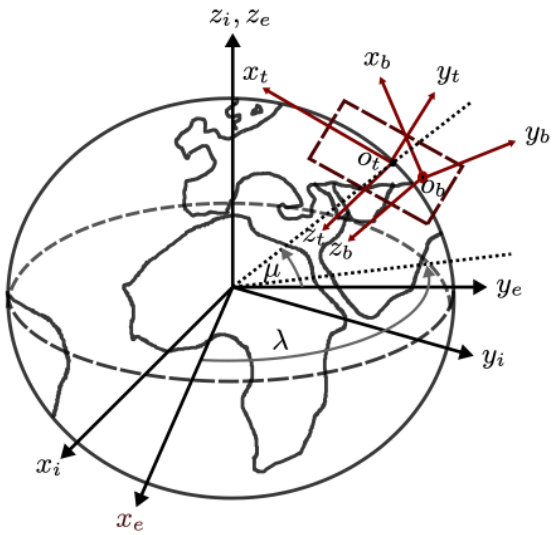

Fig. 1. Definitions of the BODY, NED (tangent), ECEF and ECI reference frames.

- $\{\cdot\}$ coordinate frames
- $\boldsymbol{S}(\cdot)$ skew symmetric matrix, $\in SS(3)$
- $\boldsymbol{z}_{bc}^{a}$ a vector $\boldsymbol{z}$, to frame $\{c\}$, relative $\{b\}$, decomposed in $\{a\}$, $\in \mathbb{R}^3$
- $\otimes$ the Hamiltonian quaternion product
- $(\cdot)^{\dagger}$ the right Moore-Penrose pseudoinverse
- $\boldsymbol{R}_{a}^{b}$ the rotation matrix from the given frame $\{a\}$ to the given frame $\{b\}$, $\in SO(3)$
- $\boldsymbol{\omega}_{ab}^{a}$ angular velocity of $\{b\}$ relative $\{a\}$, decomposed in $\{a\}$, $\in \mathbb{R}^3$
- $\boldsymbol{q}_{a}^{b}$ unit quaternion representing rotation from $\{a\}$ to $\{b\}$. $\boldsymbol{q}_{a}^{b} = (s, \boldsymbol{r}^{\intercal})^{\intercal}$ where $s \in \mathbb{R}^1$ and $\boldsymbol{r} \in \mathbb{R}^3$.
- ϕ roll
- θ pitch
- ψ yaw

B. Coordinate Reference Frames

This article employs four reference frames; The Earth Centered Inertial (ECI) frame, the Earth Centered Earth Fixed (ECEF) frame, a tangent frame equivalent of an earth-fixed North-East-Down (NED), and the BODY reference frame, denoted $\{i\}$, $\{e\}$, $\{t\}$ and $\{b\}$, respectively (see Fig. 1). ECI is an assumed inertial frame following the Earth as it orbits around the sun, where the x-axis points towards vernal equinox, the z-axis is pointing along the Earth's rotational axis and the y-axis completes the right hand frame. As for the ECEF frame, the x-axis points towards the zero meridian, the z-axis points along the Earth's rotational axis, while the y-axis completes the right hand frame. The Earth's rotation rate $\omega_{ie} = 7.292115 \cdot 10^{-5}$ rad/s is given by the WGS-84 datum. It is decomposed in the ECEF and NED frame as

$$\boldsymbol{\omega}_{ie}^{e} = \begin{pmatrix} 0 \\ 0 \\ 1 \end{pmatrix} \omega_{ie}, \quad \boldsymbol{\omega}_{ie}^{t} = \begin{pmatrix} \cos(\mu(0)) \\ 0 \\ -\sin(\mu(0)) \end{pmatrix} \omega_{ie}, \tag{1}$$

where μ is the latitude, while the longitude is denoted λ. Moreover, the navigation frame is a local Earth-fixed tangent frame, $\{t\}$, where the x-axis points towards north, the y-axis points towards east, and the z-axis points downwards. The BODY frame is fixed to the vessel. The origin of $\{b\}$ is located at the nominal center of gravity of the vessel. The x-axis is directed from aft to fore, the y-axis is directed to starboard and the z-axis points downwards.

C. Kinematic Strapdown Equations

The attitude representation most comprehensible for the user is the attitude between the BODY and the NED (tangent) frame. This is also the most intuitive representation for DP control and lever arm compensation purposes. Using a rotation matrix representation, the attitude kinematics in this article is given as

$$\dot{\boldsymbol{R}}_{b}^{t} = \boldsymbol{R}_{b}^{t}\boldsymbol{S}(\boldsymbol{\omega}_{ib}^{b}) - \boldsymbol{S}(\boldsymbol{\omega}_{it}^{t})\boldsymbol{R}_{b}^{t}, \tag{2}$$

or equivalently,

$$\dot{\boldsymbol{q}}_{b}^{t} = \frac{1}{2}\boldsymbol{q}_{b}^{t} \otimes \begin{pmatrix} 0 \\ \boldsymbol{\omega}_{ib}^{b} \end{pmatrix} - \frac{1}{2}\begin{pmatrix} 0 \\ \boldsymbol{\omega}_{it}^{t} \end{pmatrix} \otimes \boldsymbol{q}_{b}^{t}, \tag{3}$$

using the unit quaternion attitude representation. $\boldsymbol{\omega}_{it}^{t}$ is the angular rate of the navigation frame relative to the inertial frame where $\boldsymbol{\omega}_{it}^{t}$ is given as

$$\boldsymbol{\omega}_{it}^{t} = \boldsymbol{\omega}_{ie}^{t} + \boldsymbol{\omega}_{et}^{t} = \boldsymbol{\omega}_{ie}^{t}, \tag{4}$$

since a tangent frame representation of the strapdown equations is chosen, resulting in $\boldsymbol{\omega}_{et}^{t} = \boldsymbol{0}_{3\times 1}$. Moreover, $\boldsymbol{\omega}_{ib}^{b}$ is the angular rate of the navigating object relative the inertial frame, decomposed in $\{b\}$. Furthermore, from [3, Eq. (2.56)] and reference therein, the rotation matrix $\boldsymbol{R}(\boldsymbol{q}_{b}^{t}) := \boldsymbol{R}_{b}^{t}$ is obtained from $\boldsymbol{q}_{b}^{t}$ using

$$\boldsymbol{R}(\boldsymbol{q}_{b}^{t}) = \boldsymbol{I}_3 + 2s\boldsymbol{S}(\boldsymbol{r}) + 2\boldsymbol{S}(\boldsymbol{r}). \tag{5}$$

When using the tangent frame as the navigation frame, the rotational and translational motion is related with

$$\dot{\boldsymbol{p}}_{tb}^{t} = \boldsymbol{v}_{tb}^{t}, \tag{6}$$

$$\dot{\boldsymbol{v}}_{tb}^{t} = -2\boldsymbol{S}(\boldsymbol{\omega}_{ie}^{t})\boldsymbol{v}_{tb}^{t} + \boldsymbol{R}_{b}^{t}\boldsymbol{f}_{ib}^{b} + \boldsymbol{g}_{b}^{t}, \tag{7}$$

where $\boldsymbol{p}_{tb}^{t} \in \mathbb{R}^3$ is the position, relative to the tangent frame, $\boldsymbol{p}_{tb}^{t}(0) := \boldsymbol{0}_{3\times 1}$ based on $\mu(0)$ and $\lambda(0)$. Furthermore, $\boldsymbol{v}_{tb}^{t} \in \mathbb{R}^3$ is the linear velocity. It follows that $\boldsymbol{g}^{t}(\mu, \lambda) \in \mathbb{R}^3$ is the local gravity vector which may be obtained using a gravity model based on the vessel's latitude and longitude. $\boldsymbol{f}_{ib}^{b} = (\boldsymbol{R}_{b}^{t})^{\intercal}(\boldsymbol{a}_{ib}^{t} - \boldsymbol{g}_{b}^{t}) \in \mathbb{R}^3$ is the specific force decomposed in $\{\mathrm{b}\}$, where $\boldsymbol{a}_{ib}^{t}$ is the accelerations decomposed in the tangent frame, measured by the IMU. Moreover, (6)–(7) can be further extended for marine surface craft with the auxiliary variable [23]:

$$p_{tb,I}^{t} = \lim_{T\to\infty} \frac{1}{T}\int_{0}^{T} p_{z}^{t}(t)\mathrm{d}t = 0, \tag{8}$$

where I stands for *Integrated*. The augmentation is motivated by the fact that the mean vertical position of the vessel is zero over time since the wave-induced motion of the craft in heave oscillates about the mean sea level. Based on (8) we augment the strapdown equations (6)–(7) by introducing $p_{tb,I}^{t}$ as a state with

$$\dot{p}_{tb,I}^{t} = p_{tb,z}^{t}, \tag{9}$$

by integrating the vertical (down) position associated with the heave motion.

III. IMU and Ship Sensor Configuration

A. IMU and Error Sources

A strapdown IMU is a sensor unit measuring tri-axial angular velocity and tri-axial specific force of the unit in BODY frame relative the inertial frame,

$$\boldsymbol{f}^b_{\text{IMU}} = \left(f^b_x; f^b_y; f^b_z\right), \quad \boldsymbol{\omega}^b_{\text{IMU}} = \left(\omega^b_x; \omega^b_y; \omega^b_z\right),$$

where the subscripts x, y and z, denote the forward, starboard and downwards axes, respectively, in the BODY frame. In addition to the specific forces and angular velocity, each measurement is contaminated with sensor biases, errors and noise. Sensor errors may consist of nonlinearity, scale factors, cross-coupling and g-sensitivity errors, where the latter only affects the angular rate sensor's reading. In addition to internal noise sources, external noise may arise due to e.g. electrical and magnetic interference or stem from mechanical sources in the form of vibrations. In this article, we assume that error sources related to sensor nonlinearity, scale factors, misalignment, cross-coupling and g-sensitivity are compensated for in calibration, or are otherwise neglectable. Temperature-dependent sensor biases may also be compensated for by in-silico temperature sensors. For a summary on IMU error sources, see [9, Ch. 4.4].

Nevertheless, some time-varying bias instability and run-to-run and in-run instability is often present with MEMS IMUs. Therefore, we model the angular rate and accelerometer measurements as

$$\boldsymbol{\omega}^b_{\text{IMU}} = \boldsymbol{\omega}^b_{ib} + \boldsymbol{b}^b_{\text{gyro}} + \boldsymbol{w}^b_{\text{gyro}}, \tag{10}$$

$$\boldsymbol{f}^b_{\text{IMU}} = \boldsymbol{f}^b_{ib} + \boldsymbol{b}^b_{\text{acc}} + \boldsymbol{w}^b_{\text{acc}}, \tag{11}$$

where $\boldsymbol{\omega}^b_{ib}$ and $\boldsymbol{f}^b_{ib}$ are the true angular rates and specific forces, respectively. Moreover, the respective sensor biases are denoted $\boldsymbol{b}^b_{\text{gyro}}$ and $\boldsymbol{b}^b_{\text{acc}}$, while $\boldsymbol{w}^b_{\text{gyro}}$ and $\boldsymbol{w}^b_{\text{acc}}$ represent the zero mean sensor noise and vibration induced noise contained in the respective measurements. Both the angular rate/gyro and accelerometer biases are assumed slowly time-varying,

$$\dot{\boldsymbol{b}}^b_{\text{gyro}} = \boldsymbol{w}^b_{b,\text{gyro}}, \quad \dot{\boldsymbol{b}}^b_{\text{acc}} = \boldsymbol{w}^b_{b,\text{acc}}, \tag{12}$$

where $\boldsymbol{w}^b_{b,\text{gyro}}$ and $\boldsymbol{w}^b_{b,\text{acc}}$ represent small variations in the biases (zero mean).

For more detailed information on inertial sensors and inertial sensor errors, [10, Ch. 4–8] may be advised.

B. Ship Sensor Configuration

Several IMUs were installed on an offshore vessel operating in the Norwegian sea, equipped with a Rolls-Royce Marine DP system. The ship in question is owned and operated by Farstad Shipping (now Solstad Offshore). In this article we will present results obtained using ADIS16485 and STIM300 MEMS IMUs. The sensor configuration of the vessel, based on the kinematic formulation of (3), (6)–(7), (9) for fusing IMU, compass, GNSS and VVR measurements in an aided INS, was:

TABLE IV
VRU Specification

	Static roll and pitch	**Dynamic roll and pitch**	**Heave**
RMS error	0.02°	0.02°	5 cm or 5%

TABLE V
IMU specifications from manufacturer

	ADIS16485	**STIM300**
In-run Gyro Rate Bias Stability	$6.25\ \frac{\text{deg}}{\text{h}}$	$0.5\ \frac{\text{deg}}{\text{h}}$
Angular Random Walk	$0.3\ \frac{\text{deg}}{\sqrt{\text{h}}}$	$0.15\ \frac{\text{deg}}{\sqrt{\text{h}}}$
In-run Accelerometer Bias Stability	0.032 mg	0.05 mg
Velocity Random Walk	$0.023\ \frac{\text{m/s}}{\text{h}}$	$0.06\ \frac{\text{m/s}}{\text{h}}$

- 1x differential GNSS position measurement, $\boldsymbol{p}^t_{\text{GNSS}} = (p^t_x; p^t_y)$ at 1 Hz (we only use horizontal position).
- VVR: $p^t_{tb,I} = 0$, for all $t \geq 0$ at 1000 Hz. By using the VVR, other vertical references based on ranging with reduced precision due to the vertical ranging geometry, such as with GNSS-based and hydroacoustic-based PosRefs are avoided. For more details on the VVR measurement principle, see [23] and [24].
- Two different IMUs, ADIS16485 and STIM300, providing
  - Tri-axial angular rate measurements, $\boldsymbol{\omega}^b_{\text{IMU}}$
  - Tri-axial accelerometer-based specific force measurements, $\boldsymbol{f}^b_{\text{IMU}}$

  both interfaced at 1000 Hz.
- Yaw measurements from a triple-redundant gyrocompasses solution, ψ_c, at 5 Hz.

The IMU measurements are filtered with a 6th order low-pass Butterworth filter with a cutoff frequency of 5 Hz.

In addition, we use roll (ϕ) and pitch (θ) signals for comparison, obtained from a VRU at 5 Hz, see Tab. IV for specifications from the manufacturer. The specifications of the IMUs installed on the offshore vessel are presented in Tab. V.

1) Lever arm and sensor orientation: The IMUs are mounted aligned with the body frame of the vessel, and the axes of the VRU. Since the IMUs are mounted right next to the VRU the lever arms (on the decimeter level) between these sensors are considered to be negligible, considering the scale of the vessel. The lever arm from the VRU and the IMUs to the GNSS antennas is $\boldsymbol{r}^b_b = [15.73, -0.54, -32.68]^\intercal$ in meters, provided by the VRU vendor.

C. Effect of Sensor Biases and Mounting Errors on the Attitude Estimation

The IMU sensor biases has a direct effect on the attitude estimates. The gyro bias influences the attitude dynamically, while the accelerometer biases affect the attitude estimation statically. As stated in e.g. [11, Ch. 10], roll and pitch angles

may be obtained in static conditions using accelerometers or inclinometers,

$$\phi = \operatorname{atan2}(f^b_{\mathrm{IMU,y}}, f^b_{\mathrm{IMU,z}}), \tag{13}$$

$$\theta = \operatorname{atan2}(-f^b_{\mathrm{IMU,x}}, \sqrt{f^{b2}_{\mathrm{IMU,y}} + f^{b2}_{\mathrm{IMU,z}}}). \tag{14}$$

making the initialization of roll and pitch (known as leveling) susceptible to accelerometer biases. Similar to accelerometer bias, mounting (alignment) errors also contribute to static roll and pitch errors.

Akin to using accelerometers in static condition, also using them as measurement vectors in the attitude estimation of (15)–(16) may be problematic since the angular rate sensor biases and accelerometer biases are not mutually uniformly observable, [11, Ch. 11.9]. However, in most situations it is the only option to obtain a roll and pitch like reference. The theory of [16], [20] assumes zero accelerometer bias or that it is possible to compensate for it by estimation, subject to an additional persistent excitation requirement. Accelerometer bias compensation for the attitude estimation, using the bias estimate $\bar{\boldsymbol{b}}^b_{\mathrm{acc}}$, can be done statically based on calibration results or by online estimation. In this article we are applying constant accelerometer bias compensation obtained in port, based on the VRU references available, prior to the attitude observer verification scenarios. Separating the biases from mounting errors in this way is difficult, so some errors are bound to get mixed up with the biases using static methods such as (13) and (14). As presented in [35], static accelerometer bias compensation proved successful for attitude estimation for the duration of the experiments after the initial calibration due to the in-run stability of the accelerometers available.

IV. Nonlinear Observers

In this article we will compare two nonlinear attitude observers with aiding [20], [23] and without aiding [14] from a translational motion observer. An overview of the observer structure is presented in Fig. 2. Both attitude observers are based on the kinematics of (3) and the gyro bias model of (12) resulting in the observer equations,

$$\Sigma_1 : \begin{cases} \dot{\hat{\boldsymbol{q}}}^t_b = \frac{1}{2}\hat{\boldsymbol{q}}^t_b \otimes \begin{pmatrix} 0 \\ \hat{\boldsymbol{\omega}}^b_{ib} \end{pmatrix} - \frac{1}{2}\begin{pmatrix} 0 \\ \boldsymbol{\omega}^t_{it} \end{pmatrix} \otimes \hat{\boldsymbol{q}}^t_b, & \text{(15a)} \\ \hat{\boldsymbol{\omega}}^b_{ib} = \boldsymbol{\omega}^b_{\mathrm{IMU}} - \hat{\boldsymbol{b}}^b_{\mathrm{gyro}} + \hat{\boldsymbol{\sigma}}^b_{ib}, & \text{(15b)} \\ \dot{\hat{\boldsymbol{b}}}^b_{\mathrm{gyro}} = \mathrm{Proj}\left(\hat{\boldsymbol{b}}^b_{\mathrm{gyro}}, -k_I \hat{\boldsymbol{\sigma}}^b_{ib}\right), & \text{(15c)} \end{cases}$$

where the gain k_I is associated with the gyro bias estimation, and Proj denotes the gyro bias projection algorithm of [16] and the reference therein. The projection imposes a bound on $\hat{\boldsymbol{b}}^b_{\mathrm{gyro}}$ to a compact set. The difference between the two observers lies in the injection term, $\hat{\boldsymbol{\sigma}}^b_{ib}$, given as

$$\hat{\boldsymbol{\sigma}}^b_{ib} = k_1 \underline{\boldsymbol{v}}^b_1 \times \boldsymbol{R}^{\mathsf{T}}(\hat{\boldsymbol{q}}^t_b)\underline{\boldsymbol{v}}^t_1 + k_2 \underline{\boldsymbol{v}}^b_2 \times \boldsymbol{R}^{\mathsf{T}}(\hat{\boldsymbol{q}}^t_b)\underline{\boldsymbol{v}}^t_2, \tag{16}$$

where $\underline{\boldsymbol{v}}^b_1$ and $\underline{\boldsymbol{v}}^b_2$ are the measurement vectors and $\underline{\boldsymbol{v}}^t_1$ and $\underline{\boldsymbol{v}}^t_2$ are the reference vectors, calculated using

$$\underline{\boldsymbol{v}}^b_1 = \underline{\boldsymbol{f}}^b, \quad \underline{\boldsymbol{v}}^b_2 = \underline{\boldsymbol{f}}^b \times \underline{\boldsymbol{c}}^b,$$
$$\underline{\boldsymbol{v}}^t_1 = \underline{\boldsymbol{f}}^t, \quad \underline{\boldsymbol{v}}^t_2 = \underline{\boldsymbol{f}}^t \times \underline{\boldsymbol{c}}^t.$$

TABLE VI
NLO reference vectors configuration

	Vector $\underline{\boldsymbol{c}}^t$	Vector $\underline{\boldsymbol{f}}^t$
NLO A	Unit vector North	$-\boldsymbol{g}^t_b/\|-\boldsymbol{g}^t_b\|_2$
NLO B	Unit vector North	$\hat{\boldsymbol{f}}^t_{ib}/\|\hat{\boldsymbol{f}}^t_{ib}\|_2$ through feedback from VVR and PosRef injection

An overview of the main differences of NLO A and B can be found in Tab. VI. For both, $\underline{\boldsymbol{c}}^b = (\cos(\psi_c); -\sin(\psi_c); 0)$ and $\underline{\boldsymbol{c}}^t = (1; 0; 0)$ as posed in [22]. Both $\underline{\boldsymbol{c}}^b$ and $\underline{\boldsymbol{c}}^t$ are naturally normalized. By using normalized measurement/reference vector pairs, the gains k_1 and k_2 can be considered as the NLO's complementary filter cut-off frequencies having unit rad/s. Hence, for motion frequencies higher than k_1 and k_2, the angular rate measurements are the primary sources of attitude information, while for frequencies lower than k_1 and k_2, the respective measurement vectors are the primary sources of attitude information.

A. Nonlinear Attitude Observer A

For attitude observer A, $\hat{\boldsymbol{\sigma}}^b_{ib,A}$ is implemented with $\underline{\boldsymbol{f}}^b$ and $\underline{\boldsymbol{f}}^t$ based on the injection term of [14] with

$$\underline{\boldsymbol{f}}^b = \frac{\boldsymbol{f}^b_{\mathrm{IMU}} - \bar{\boldsymbol{b}}^b_{\mathrm{acc}}}{\|\boldsymbol{f}^b_{\mathrm{IMU}} - \bar{\boldsymbol{b}}^b_{\mathrm{acc}}\|_2}, \quad \underline{\boldsymbol{f}}^t = \frac{-\boldsymbol{g}^t_b}{\|-\boldsymbol{g}^t_b\|_2}, \tag{17}$$

where the local gravity vector is utilized as reference vector based on the assumption that the specific force in the navigation frame is dominated by $-\boldsymbol{g}^t_b$.

B. Nonlinear Attitude Observer B

Regarding attitude observer B, the reference vector $\underline{\boldsymbol{f}}^t$, in the calculation of $\hat{\boldsymbol{\sigma}}^b_{ib,B}$ is chosen as

$$\underline{\boldsymbol{f}}^t = \frac{\mathrm{sat}_{M_f}(\hat{\boldsymbol{f}}^t_{ib})}{\|\mathrm{sat}_{M_f}(\hat{\boldsymbol{f}}^t_{ib})\|_2}, \tag{18}$$

where $\hat{\boldsymbol{f}}^t_{ib}$ is estimated using a modified version of the feedback-interconnected observer framework [20], using the Translational Motion Observers (TMO) of [22], [23], where the VVR aiding concept is applied. Moreover, by providing the specific force estimate $\hat{\boldsymbol{f}}^t_{ib}$, to Σ_1, the attitude estimate is potentially more accurate when the vessel is accelerated than it is when using $-\boldsymbol{g}^t_b$ as reference vector. $\hat{\boldsymbol{f}}^t_{ib}$, provided to attitude observer B, is estimated using the TMO Σ_2 (see Fig. 2 and below), which has injection from a PosRef in addition to the VVR measurement. The TMO used to estimate $\hat{\boldsymbol{f}}^t_{ib}$ used

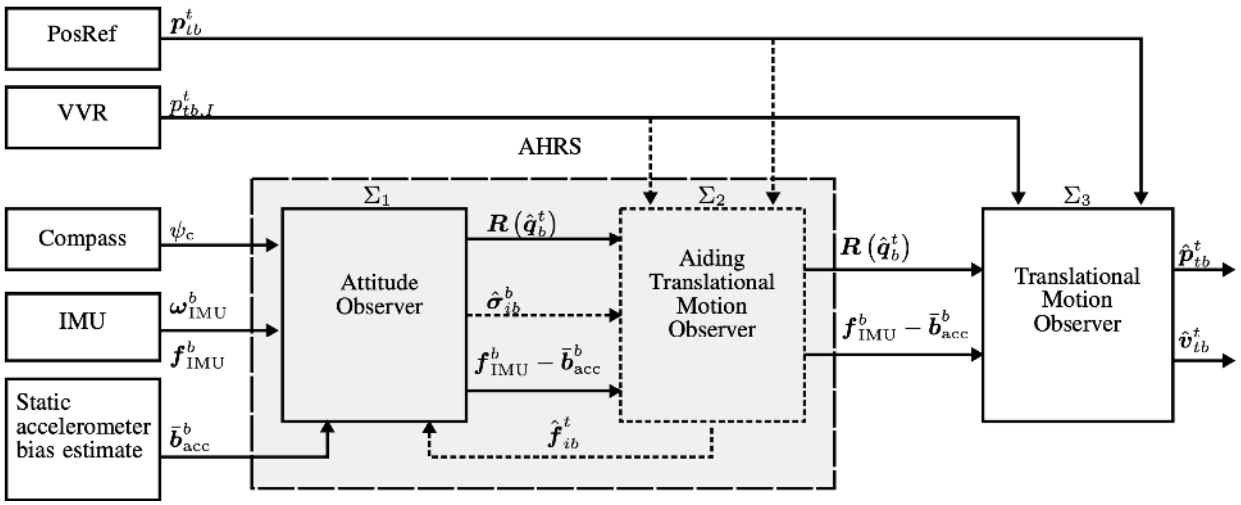

Fig. 2. Observer structure for strapdown inertial navigation. Depending on configuration, the Attitude and Heading Reference System (AHRS) may be aided internally by a Translational Motion Observer, itself aided by PosRefs and VVR measurements.

by NLO B takes the form of

$$\Sigma_2 : \begin{cases} \dot{\hat{p}}^t_{tb,I} = \hat{p}^t_{tb,z} + \vartheta K_{pIpI} \tilde{p}^t_{tb,I}, & \text{(19a)} \\ \dot{\hat{\boldsymbol{p}}}^t_{tb} = \hat{\boldsymbol{v}}^t_{tb} \\ \qquad + \vartheta^2 \begin{pmatrix} \boldsymbol{0}_{2\times 1} \\ K_{ppI} \end{pmatrix} \tilde{p}^t_{tb,I} + \vartheta \begin{pmatrix} \boldsymbol{K}_{pp} \\ 0 \quad 0 \end{pmatrix} \tilde{\boldsymbol{p}}^t_{tb}, & \text{(19b)} \\ \dot{\hat{\boldsymbol{v}}}^t_{tb} = -2\boldsymbol{S}(\boldsymbol{\omega}^t_{ie})\boldsymbol{v}^t_{tb} + \hat{\boldsymbol{f}}^t_{ib} + \boldsymbol{g}^t_b \\ \qquad + \vartheta^3 \begin{pmatrix} \boldsymbol{0}_{2\times 1} \\ K_{vpI} \end{pmatrix} \tilde{p}^t_{tb,I} + \vartheta^2 \begin{pmatrix} \boldsymbol{K}_{vp} \\ 0 \quad 0 \end{pmatrix} \tilde{\boldsymbol{p}}^t_{tb}, & \text{(19c)} \\ \dot{\boldsymbol{\xi}}^t_{ib} = -\boldsymbol{R}(\hat{\boldsymbol{q}}^t_b)\boldsymbol{S}(\hat{\boldsymbol{\sigma}}^b_{ib,B}) \left(\boldsymbol{f}^b_{\text{IMU}} - \bar{\boldsymbol{b}}^b_{\text{acc}} \right) \\ \qquad + \vartheta^4 \begin{pmatrix} \boldsymbol{0}_{2\times 1} \\ K_{\xi pI} \end{pmatrix} \tilde{p}^t_{tb,I} + \vartheta^3 \begin{pmatrix} \boldsymbol{K}_{\xi p} \\ 0 \quad 0 \end{pmatrix} \tilde{\boldsymbol{p}}^t_{tb}, & \text{(19d)} \\ \hat{\boldsymbol{f}}^t_{ib} = \boldsymbol{R}(\hat{\boldsymbol{q}}^t_b) \left(\boldsymbol{f}^b_{\text{IMU}} - \bar{\boldsymbol{b}}^b_{\text{acc}} \right) + \boldsymbol{\xi}^t_{ib}, & \text{(19e)} \end{cases}$$

where $\tilde{p}^t_{tb,I} = p^t_{tb,I} - \hat{p}^t_{tb,I}$, $\tilde{\boldsymbol{p}}^t_{tb} = \boldsymbol{p}^t_{\text{GNSS}} - (\hat{p}^t_{tb,x}; \hat{p}^t_{tb,y})$. $K_{[\cdot]pI}$ and $\boldsymbol{K}_{[\cdot]p}$ are fixed gains, while $\vartheta \geq 1$ is a tuning parameter used to guarantee stability. Since the VVR provides $p^t_I = 0$ for all $t \geq 0$, the vertical estimates of Σ_2 are self contained regardless of GNSS precision and accuracy or GNSS position fix. The gains may be chosen such that the feedback interconnection $\Sigma_1 - \Sigma_2$ possesses uniform semiglobal exponential stability [23].

In state-space form, the aiding TMO is represented as:

$$\dot{\hat{\boldsymbol{x}}}_a = \boldsymbol{A}_a \hat{\boldsymbol{x}}_a + \boldsymbol{B}_a \boldsymbol{u}_a + \vartheta \boldsymbol{L}^{-1}_\vartheta \boldsymbol{K}_a \boldsymbol{E}_\vartheta \left(\boldsymbol{y} - \boldsymbol{C} \hat{\boldsymbol{x}}_a \right) + \boldsymbol{D}_a \quad (20)$$

with the state space, measurements and input vectors

$$\begin{aligned} \hat{\boldsymbol{x}}_a &= \left(\hat{p}^t_{tb,I}; \hat{\boldsymbol{p}}^t_{tb}; \hat{\boldsymbol{v}}^t_{tb}; \hat{\boldsymbol{\xi}}^t_{ib} \right), \\ \boldsymbol{y} &= \left(p^n_I; \boldsymbol{p}^t_{\text{GNSS}} \right), \\ \boldsymbol{u} &= \left(\boldsymbol{f}^b_{\text{IMU}} - \bar{\boldsymbol{b}}^b_{\text{acc}}; -\boldsymbol{S}(\hat{\boldsymbol{\sigma}})(\boldsymbol{f}^b_{\text{IMU}} - \bar{\boldsymbol{b}}^b_{\text{acc}}) \right), \end{aligned}$$

and matrices and vectors,

$$\begin{aligned} \boldsymbol{A}_a &= \begin{pmatrix} 0 & \begin{pmatrix} 0 & 0 & 1 \end{pmatrix} & \boldsymbol{0}_{1\times 3} & \boldsymbol{0}_{1\times 3} \\ \boldsymbol{0}_{3\times 1} & \boldsymbol{0}_{3\times 3} & \boldsymbol{I}_3 & \boldsymbol{0}_{3\times 3} \\ \boldsymbol{0}_{3\times 1} & \boldsymbol{0}_{3\times 3} & \boldsymbol{0}_{3\times 3} & \boldsymbol{I}_3 \\ \boldsymbol{0}_{3\times 1} & \boldsymbol{0}_{3\times 3} & \boldsymbol{0}_{3\times 3} & \boldsymbol{0}_{3\times 3} \end{pmatrix}, \\ \boldsymbol{B}_a &= \begin{pmatrix} \boldsymbol{0}_{1\times 3} & \boldsymbol{0}_{1\times 3} \\ \boldsymbol{0}_{3\times 3} & \boldsymbol{0}_{3\times 3} \\ \boldsymbol{R}(\hat{\boldsymbol{q}}^t_b) & \boldsymbol{0}_{3\times 3} \\ \boldsymbol{0}_{3\times 3} & \boldsymbol{R}(\hat{\boldsymbol{q}}^t_b) \end{pmatrix}, \\ \boldsymbol{C}_a &= \begin{pmatrix} \boldsymbol{I}_3 & \boldsymbol{0}_{3\times 7} \end{pmatrix}, \\ \boldsymbol{D}_a &= \begin{pmatrix} 0; & \boldsymbol{0}_{3\times 1}; & -2\boldsymbol{S}(\boldsymbol{\omega}^t_{ie})\boldsymbol{v}^t_{tb} + \boldsymbol{g}^t_b; & \boldsymbol{0}_{3\times 1} \end{pmatrix}, \\ \boldsymbol{K}_a &= \begin{pmatrix} K_{pIpI} & \boldsymbol{0}_{1\times 2} \\ \boldsymbol{0}_{2\times 1} & \boldsymbol{K}_{pp} \\ K_{ppI} & \boldsymbol{0}_{1\times 2} \\ \boldsymbol{0}_{2\times 1} & \boldsymbol{K}_{vp} \\ K_{vpI} & \boldsymbol{0}_{1\times 2} \\ \boldsymbol{0}_{2\times 1} & \boldsymbol{K}_{\xi p} \\ K_{\xi pI} & \boldsymbol{0}_{1\times 2} \end{pmatrix}, \\ \boldsymbol{L}_\vartheta &= \text{blockdiag} \left(1, \frac{1}{\vartheta}\boldsymbol{I}_3, \frac{1}{\vartheta^2}\boldsymbol{I}_3, \frac{1}{\vartheta^3}\boldsymbol{I}_3 \right), \\ \boldsymbol{E}_\vartheta &= \boldsymbol{C}_a \boldsymbol{L}_\vartheta \boldsymbol{C}^\dagger_a, \end{aligned}$$

where $\boldsymbol{E}_\vartheta$ satisfies $\boldsymbol{E}_\vartheta \boldsymbol{C}_a = \boldsymbol{C}_a \boldsymbol{L}_\vartheta$ such that the semiglobal exponential stability follows from [22].

C. Translational Motion Observer

Even though the gyro and accelerometer biases are not mutually uniformly observable, [11, Ch. 11.9], without the vessel accelerating and rotating, some accelerometer bias compensation has to be performed in order to obtain an INS with reasonable dead reckoning capabilities. For $\Sigma_1 - \Sigma_2$, a fixed pre-compensated accelerometer bias $\bar{\boldsymbol{b}}^b_{\text{acc}}$ is applied for attitude estimation. However, some accelerometer errors may be present owing to some in-run bias instability, w.r.t. Tab. V. To atone for this, we create a new TMO including an estimate of the residual accelerometer bias $\hat{\boldsymbol{b}}^b_{\text{acc}}$, inspired

by the observer of [3, Ch. 11.5.1]. Observer Σ_3 for additional accelerometer bias estimation can be described as follows:

$$\dot{\hat{\boldsymbol{x}}} = \boldsymbol{A}\hat{\boldsymbol{x}} + \boldsymbol{B}\boldsymbol{u} + \boldsymbol{K}\left(\boldsymbol{y} - \boldsymbol{C}\hat{\boldsymbol{x}}\right) + \boldsymbol{D} \tag{21}$$

with $\hat{\boldsymbol{x}} = \left(p^t_{tb,I}; \hat{\boldsymbol{p}}^t_{tb}; \hat{\boldsymbol{v}}^t_{tb}; \hat{\boldsymbol{b}}^b_{\text{acc}}\right)$,
$\boldsymbol{y} = (p^n_I; \boldsymbol{p}^t_{\text{GNSS}})$ and $\boldsymbol{u} = \boldsymbol{f}^b_{\text{IMU}} - \bar{\boldsymbol{b}}^b_{\text{acc}}$, resulting in

$$\boldsymbol{A} = \begin{pmatrix} 0 & \begin{pmatrix}0 & 0 & 1\end{pmatrix} & \boldsymbol{0}_{1\times3} & \boldsymbol{0}_{1\times3} \\ \boldsymbol{0}_{3\times1} & \boldsymbol{0}_{3\times3} & \boldsymbol{I}_3 & \boldsymbol{0}_{3\times3} \\ \boldsymbol{0}_{3\times1} & \boldsymbol{0}_{3\times3} & \boldsymbol{0}_{3\times3} & -\boldsymbol{R}(\hat{\boldsymbol{q}}^t_b) \\ \boldsymbol{0}_{3\times1} & \boldsymbol{0}_{3\times3} & \boldsymbol{0}_{3\times3} & \boldsymbol{0}_{3\times3} \end{pmatrix},$$

$$\boldsymbol{B} = \begin{pmatrix} \boldsymbol{0}_{1\times3} \\ \boldsymbol{0}_{3\times3} \\ \boldsymbol{R}(\hat{\boldsymbol{q}}^t_b) \\ \boldsymbol{0}_{3\times3} \end{pmatrix},$$

$$\boldsymbol{C} = \begin{pmatrix} \boldsymbol{I}_3 & \boldsymbol{0}_{3\times7} \end{pmatrix},$$

$$\boldsymbol{D} = \begin{pmatrix} 0; & \boldsymbol{0}_{3\times1}; & -2\boldsymbol{S}(\boldsymbol{\omega}^t_{ie})\boldsymbol{v}^t_{tb} + \boldsymbol{g}^t_b; & \boldsymbol{0}_{3\times1} \end{pmatrix},$$

Considering $\boldsymbol{R}(\hat{\boldsymbol{q}}^t_b)$ as an external signal to Σ_3, $\boldsymbol{A}$ is treated as time-varying and the TMO's error dynamics is rendered exponentially stable by employing a Riccati-equation and gain similar to the Kalman-Bucy filter [37],

$$\boldsymbol{K} = \boldsymbol{P}\boldsymbol{C}^\intercal\boldsymbol{R}^{-1}, \tag{22}$$

$$\dot{\boldsymbol{P}} = \boldsymbol{A}\boldsymbol{P} + \boldsymbol{P}\boldsymbol{A}^\intercal - \boldsymbol{K}\boldsymbol{R}\boldsymbol{K}^\intercal + \boldsymbol{G}\boldsymbol{Q}\boldsymbol{G}^\intercal. \tag{23}$$

$\boldsymbol{Q}$ and $\boldsymbol{R}$ are covariance matrices chosen according to sensor noise and desired tuning, see Section V. Furthermore, the process noise disruption matrix is chosen to be

$$\boldsymbol{G} = \begin{pmatrix} \boldsymbol{0}_{1\times3} & \boldsymbol{0}_{1\times3} \\ \boldsymbol{0}_{3\times3} & \boldsymbol{0}_{3\times3} \\ \boldsymbol{R}(\hat{\boldsymbol{q}}^t_b) & \boldsymbol{0}_{3\times3} \\ \boldsymbol{0}_{3\times3} & \boldsymbol{I}_3 \end{pmatrix}, \tag{24}$$

such that the process noise associated with the accelerometer in $\boldsymbol{Q}$ is related to the navigation frame, $\{t\}$, through $\boldsymbol{R}(\hat{\boldsymbol{q}}^t_b)$. The actual implementation of the observer is done in discrete time, as in for instance [9], using the discrete time versions of the Riccati equation and Kalman gain.

V. Observer tuning

Observer tuning is usually dependent on both the properties of the sensors and the system in which one is trying to estimate states. In our case, we found that external noise sources, i.e. vibrations, dominate those originating internally. Therefore, we opted to use the same observer tuning for both the ADIS16485 and STIM300. For Σ_1 we used the gains $k_1 = 0.1, k_2 = 0.1, k_I = 0.05$.

For Σ_2, the parameter $\vartheta = 1$ was chosen. For the gains $K_{[\cdot]p_I}$ and $\boldsymbol{K}_{[\cdot]p}$, we employed the continuous-time steady-state Riccati equation, similar to the Kalman-Bucy filter [37], and akin to Σ_3,

$$\boldsymbol{K}_a = \boldsymbol{P}_{a,\infty}\boldsymbol{C}_a^\intercal\boldsymbol{R}_a^{-1}$$
$$\boldsymbol{0} = \boldsymbol{A}_a\boldsymbol{P}_{a,\infty} + \boldsymbol{P}_{a,\infty}\boldsymbol{A}_a - \boldsymbol{K}_a\boldsymbol{R}_a\boldsymbol{K}_a^\intercal + \boldsymbol{B}_a\boldsymbol{Q}_a\boldsymbol{B}_a^\intercal$$

using the following covariance matrices for process and measurement noise

$$\boldsymbol{Q}_a = \text{blockdiag}(0.1^2 \cdot \boldsymbol{I}_3,\ 0.15^2 \cdot \boldsymbol{I}_3),$$
$$\boldsymbol{R}_a = \text{blockdiag}(35^2,\ 2^2 \cdot \boldsymbol{I}_2),$$

where the first element of $\boldsymbol{Q}_a$ is the variance associated with the input $\boldsymbol{f}^b_{\text{IMU}}$, and the second element is associated with the cross product of $\hat{\boldsymbol{\sigma}}$ and $\boldsymbol{f}^b_{\text{IMU}}$ as seen in (19d). The first element of $\boldsymbol{R}_a$ is a value representing VVR measurement uncertainty, and the second element is the GNSS horizontal measurement variance. This resulted in the the following gains:

$$K_{p_Ip_I} = 0.6368,$$
$$K_{pp_I} = 0.2028, \boldsymbol{K}_{pp} = 0.7950 \cdot \boldsymbol{I}_2,$$
$$K_{vp_I} = 0.0378, \boldsymbol{K}_{vp} = 0.3160 \cdot \boldsymbol{I}_2,$$
$$K_{\xi p_I} = 0.0035, \boldsymbol{K}_{\xi p} = 0.0612 \cdot \boldsymbol{I}_2.$$

For Σ_3 we chose the following covariance matrices to go with the Riccati equation:

$$\boldsymbol{Q} = \text{blockdiag}(0.1^2\boldsymbol{I}_3,\ 0.001^2 \cdot \boldsymbol{I}_3).$$
$$\boldsymbol{R} = \text{blockdiag}(20^2,\ 2^2 \cdot \boldsymbol{I}_2).$$

As for Σ_2, the first element of $\boldsymbol{Q}$ is the variance associated with $\boldsymbol{f}^b_{\text{IMU}}$, but the second element is the process noise of the $\hat{\boldsymbol{b}}^b_{\text{acc}}$ state. $\boldsymbol{R}$ represents exactly the same as $\boldsymbol{R}_a$, albeit tuned a bit differently for the VVR measurement because of the different dynamics of Σ_2 and Σ_3.

All matrices are tuned in continuous time, and then converted to discrete time equivalents in the actual implementation, see for instance [9] for methods for discretization.

VI. Full-scale Testing: Attitude

In this section, we present the results of the attitude estimation using two distinct attitude observers and two particular MEMS IMUs, during two different operations undertaken by the offshore vessel. The first operation is station keeping during DP. The second is a maneuvering operation, where the vessel changes heading while surging forward. Plots of the respective path tracks over two hours are shown in Fig. 3. The attitude estimation is evaluated using the mean error, Root-Mean-Square Error (RMSE) and Cumulative Absolute Error (CAE) metrics, using the onboard VRU as reference. Also, a comparison with the output of NavLab [38] is provided. NavLab is a navigation software suite based on the EKF, and has been applied in industry and defense on a wide range of systems, maritime and otherwise. The metrics for all estimators were evaluated for a 90-minutes data set. We do not generate statistics for yaw estimation error, as this is somewhat meaningless exercise considering that the gyrocompass, which is our only reference for heading, is also aiding our attitude observers.

A. DP

An excerpt of the attitude estimates obtained using the STIM300 IMU and NLO B in DP is shown in Fig. 4a. The estimation errors relative the VRU and gyrocompass

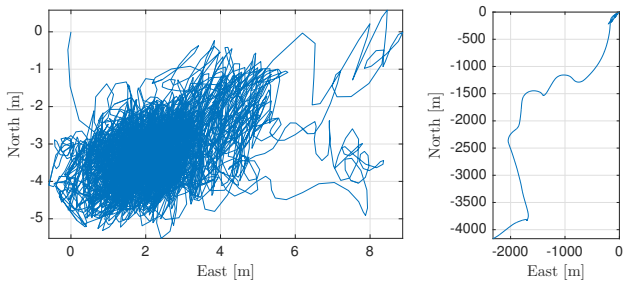

(a) Dynamic Positioning (b) Maneuvering

Fig. 3. Two North-East tracks depicting operational situations used to evaluate the attitude estimation performance. The path tracks are obtained from the onboard GNSS.

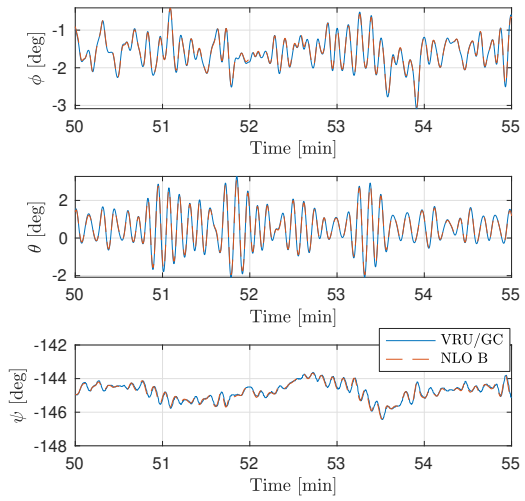

(a) Attitude estimates: Roll, pitch and yaw.

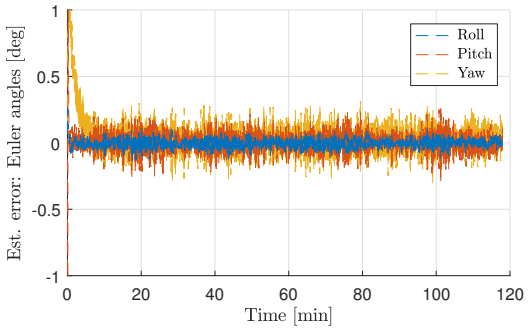

(b) Attitude estimation error: Roll, pitch and yaw.

Fig. 4. Sample attitude estimation using NLO B and STIM300.

measurements over two hours are shown in Fig. 4b. The statistics obtained using the attitude estimators in DP are presented in Tab. VII. One can see that the choice of estimator to perform the attitude estimation in DP is more important than the choice of sensor, at least when it comes to our selection of IMUs. It is evident from the results that both the RMSE and CAE is improved using NLO B and NavLab compared to the results obtained with NLO A. This is particularly noticeable in roll. The mean errors are approximately the same, where the differences are on such a scale that the practical effects of such errors, for instance in lever arm compensation, are negligible. For NavLab, larger differences are observed between the IMUs than is the case for the NLOs. This could mean that the tuning of NavLab is more sensor dependent than the NLOs.

B. Maneuvering

The statistics obtained using attitude estimators during maneuvering are presented in Tab. VIII. Results comparable to what were obtained in DP, are achieved during the maneuvers as shown in Tab VIII. NLO B and NavLab outperform NLO A considering RMSE and CAE in roll and pitch, but not as much as in the DP case. As opposed to the DP case, here NavLab was in line with the other two estimators and yielded virtually no difference in output between the two sensors.

C. Discussion

The results obtained during DP and maneuvering gave approximately similar results for both IMUs. The two different NLOs however provided varied results when compared to the onboard VRUs.

During both test cases, the attitude estimation errors compared to the VRU were smaller using NLO B, compared to using NLO A, particularly in roll. NLO A has a static specific force injection, (see Sec. IV and Tab. VI) using $-\boldsymbol{g}_b^t$ as reference vector. However, $-\boldsymbol{g}_b^t$ is not equal to $\boldsymbol{f}_{ib}^t$, even in DP, due to the wave-induced motions of the vessel. The positive effect of using $\hat{\boldsymbol{f}}_{ib}^t$ as reference vector is considerable, as expected from the results of [23], due to the kinematic coupling between roll, pitch and heave obtained using VVR as vertical reference in TMO Σ_2. However, in light of this, a peculiar result is that the difference between NLO A and B *decreases* from DP to maneuvering even though the dynamics of the system apparently increase. This may be because the increase in dynamics is mainly in the horizontal plane, where the quality of the GNSS position measurement matters more and the VVR impact is minimal.

The performance of NLO B was comparable to what we achieved with NavLab. In contrast to the Kalman filter, the NLOs used here are not designed with optimality in mind, as in minimum variance, but rather stability and guarantees of convergence. Still, we managed to get similar stationary performance for attitude estimation compared to an EKF-based solution of NavLab. This reaffirms previous results on GNSS/INS-integration using NLOs [21].

Compared to what was achieved in [35], we see an improvement of the nonlinear attitude estimation results. This is mostly due to the low-pass filtering of IMU data, which was not done in [35]. Low-pass filtering may be beneficial for the nonlinear observers employed here, which are derived without the assumption of sensor and vibration noise.

Since accelerometer measurements dominate the roll and pitch estimates at frequencies below the NLO's internal cut-off frequency k_1, the mean error over time is dependent on the accelerometer sensor biases. However, the accelerometer biases are not estimated online for the NLO's, but rather calculated as a constant in port as much as three days before the second vessel operation presented. As both IMUs give

TABLE VII
ATTITUDE ERROR STATISTICS IN DP

	NavLab		NLO A		NLO B	
	ADIS16485	STIM300	ADIS16485	STIM300	ADIS16485	STIM300
Roll mean error [deg]	-0.0193	-0.0094	0.0036	0.0003	-0.0007	-0.0044
Pitch mean error [deg]	0.0463	0.0063	0.0090	0.0070	0.0047	0.0016
Roll RMSE [deg]	0.0417	0.0287	0.1113	0.1151	0.0363	0.0299
Pitch RMSE [deg]	0.0813	0.0628	0.1080	0.1071	0.0670	0.0649
Roll CAE [deg]	881.89	610.79	2361.8	2442.7	759.80	628.99
Pitch CAE [deg]	1731.1	1233.3	2254.9	2239.7	1406.0	1357.5

TABLE VIII
ATTITUDE ERROR STATISTICS DURING MANEUVERING

	NavLab		NLO A		NLO B	
	ADIS16485	STIM300	ADIS16485	STIM300	ADIS16485	STIM300
Roll mean error [deg]	-0.0345	-0.0301	-0.0089	-0.0134	-0.0080	-0.0115
Pitch mean error [deg]	0.0311	0.0081	-0.0245	-0.0041	-0.0188	0.0022
Roll RMSE [deg]	0.0847	0.0817	0.1102	0.1122	0.0870	0.0848
Pitch RMSE [deg]	0.1078	0.1154	0.1161	0.1139	0.1113	0.1193
Roll CAE [deg]	1613.3	1433.3	2442.6	2484.0	1636.3	1575.8
Pitch CAE [deg]	2135.6	2123.5	2638.6	2582.6	2446.2	2500.2

good performance with regards to mean roll and pitch error, one can conclude that the accelerometer biases do not vary by much and the sensors are highly in-run stable in the environment they are located.

It should also be emphasized that we compared the NLOs' performance to the VRU's equivalent signals and not to absolute truth, revisit Tab. IV for the VRU specifications. Hence, there may exist situations where the combination of IMUs and NLOs provide more accurate estimates than the VRU.

VII. FULL-SCALE TESTING: HEAVE

A. DP and maneuvering

Heave estimation is carried out on the exact same data sets as in Sec. VI, and using the same metrics. Since NavLab does not provide the VVR functionality, it will not be used for comparison in this section. A selection of the heave estimates obtained using the STIM300 and Σ_2 and Σ_3 is shown in Fig. 5. The heave estimation error statistics obtained using the same observers are presented in Tabs. IX–X.

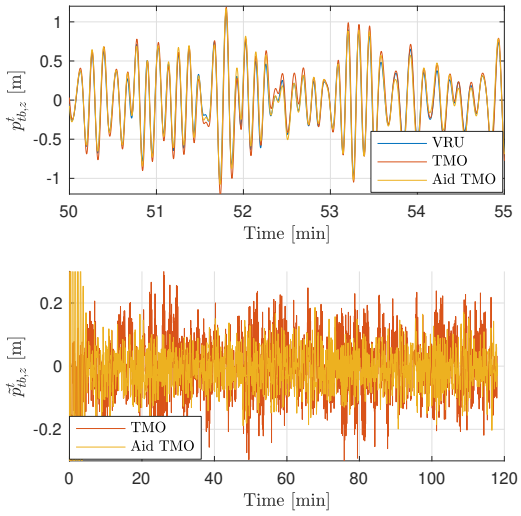

Fig. 5. Sample heave estimation and estimation error in DP using Σ_2 (yellow) and Σ_3 (red) vs. the onboard VRU (blue).

B. Discussion

Considering the heave estimation performance, this appears to be better when using the ADIS16485 as IMU. Between Σ_2 and Σ_3, there appears to be some differences in favor of Σ_2. While the attitude estimates showed practically no difference between the IMUs, the use of ADIS16485 gave better heave estimates than those obtained with STIM300, with the method used. This might be due to the ADIS16485's accelerometer having better velocity-random walk characteristics than the STIM300. Also, it should be mentioned that the STIM300 unit provided by Sensonor, is an engineering sample. Such units are made for testing and do not necessarily fulfill all of the specifications in the datasheet under all environmental conditions. Therefore, we cannot guarantee that the results obtained is representative for a commercially available STIM300. Generally for the heave estimation results, they might be improved with a tuning emphasizing heave specifically, or using alternative algorithms, such as in [24]. Even though low-pass filtering improved the attitude estimation compared to [35], we do not see the same consistent improvements compared to the corresponding results for heave.

TABLE IX
HEAVE ERROR STATISTICS IN DP

	Σ_2		Σ_3	
	ADIS16485	STIM300	ADIS16485	STIM300
Mean heave error [cm]	-0.6511	-0.6005	0.2288	0.1339
RMSE heave [cm]	5.7766	10.523	8.0644	10.274
CAE heave [cm]	1215.0	2207.3	1706.2	2112.6

TABLE X
HEAVE ERROR STATISTICS DURING MANEUVERING

	Σ_2		Σ_3	
	ADIS16485	STIM300	ADIS16485	STIM300
Mean heave error [cm]	-0.2982	-0.2689	0.3831	0.7008
RMSE heave [cm]	6.3318	9.8799	8.5277	12.308
CAE heave [cm]	1462.5	2275.0	1907.4	2699.1

VIII. FULL-SCALE TESTING OF DEAD RECKONING CAPABILITY IN DP

In this section, the evaluation of the dead reckoning properties in light of fault detection using the ADIS16485 and STIM300 is presented. The dead reckoning performance evaluation is carried out with data collected in a DP operation whose GNSS track is shown in Fig. 3a.

First, the heading dead reckoning performance when using the IMUs available is discussed, and illustrated with an example. Then, the position dead reckoning performance during the particular DP operation is evaluated, applying both IMUs and NLO A with Σ_3.

The resulting statistics are based on running the estimators 60 times on subsets of the DP dataset with an incremental increase in initial time for each subset. For heading dead reckoning performance evaluation the datasets are 75 minutes long, allowing for 15 minutes of estimator settling time and a 60 minute evaluation window. The duration is chosen to compare the performance with the sensor specifications, while the amount of runs is chosen in order to have sufficient evaluation samples while still maintaining separation of the starting time of the datasets. For position, the same settling time is chosen, but we use only 10 minutes of evaluation time as the position is expected to drift substantially more than the heading in dead reckoning.

A. Heading Angle Dead Reckoning Capabilities

The heading angle dead reckoning capabilities using the IMUs available were found to be in compliance with the IMUs' angular rate specifications, presented in Tab. V. A total of 60 one-hour-long heading evolutions of the absolute yaw angle error

$$|\tilde{\psi}| = |\psi_c - \hat{\psi}|, \tag{25}$$

compared to the ship gyrocompass measurements for both sensors, are shown in Fig. 6. The dead reckoning was carried out with NLO B, by disabling the observer injection from the gyrocompass by setting $k_2 = 0$, after an observer initialization time of 15 minutes. In addition, the average heading error, of the 60 runs, is highlighted in Fig. 6. Examples of typical angular rate bias estimates are shown in Fig. 7, exhibiting that the STIM300's biases are more in-run stable than those of the ADIS16485.

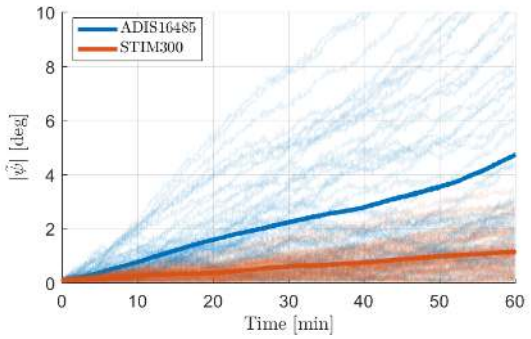

Fig. 6. Dead reckoning performance in yaw obtained using the ADIS16485 and STIM300 IMUs. Highlighted graph indicates average error.

B. Position Read Reckoning Capabilities

Evaluation of the dead reckoning capabilities in position is similar yet more elaborate than for heading since the theoretical growth of errors are a combination of higher order terms, [9, Ch. 5.7], as opposed to linear growth for heading. In order to obtain statistically significant results related to the position drift while performing dead reckoning, each combination of IMU and NLO was evaluated 60 times by comparing the errors accumulated when disabling GNSS feedback after $t = 15$ minutes, and then continuing the estimation for 10 minutes. The evaluation is done by taking the norm of the difference between the horizontal components of $\boldsymbol{p}^t_{\text{GNSS}}$ and $\hat{\boldsymbol{p}}^t_{\text{GNSS}}$, defined $\tilde{\boldsymbol{p}}^t_{\text{GNSS}} := \boldsymbol{p}^t_{\text{GNSS}} - \hat{\boldsymbol{p}}^t_{\text{GNSS}}$ where,

$$\hat{\boldsymbol{p}}^t_{\text{GNSS}} = \hat{\boldsymbol{p}}^t_{tb} + \boldsymbol{R}(\hat{\boldsymbol{q}}^t_b)\boldsymbol{r}^b_b, \tag{26}$$

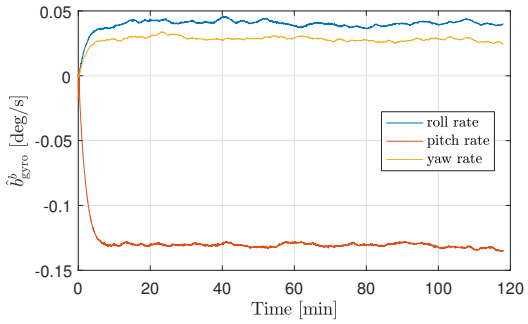

(a) Typical angular rate bias estimates of the ADIS16485.

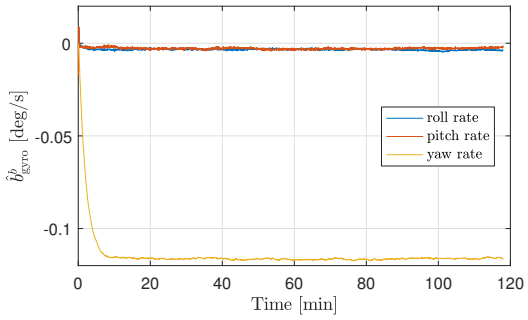

(b) Typical angular rate bias estimates of the STIM300.

Fig. 7. Typical angular rate bias estimates for the two different IMUs

with $\boldsymbol{r}_b^b$ being the lever arm from the IMU to the GNSS antenna position such that

$$\begin{aligned}\|\tilde{\boldsymbol{p}}^t_{\text{GNSS}}\|_2 &= \|\boldsymbol{p}^t_{tb} + \boldsymbol{R}^t_b \boldsymbol{r}^b_b - \hat{\boldsymbol{p}}^t_{tb} - \boldsymbol{R}(\hat{\boldsymbol{q}}^t_b)\boldsymbol{r}^b_b\|_2, \\ &= \|\tilde{\boldsymbol{p}}_{tb} + \left(\boldsymbol{R}^t_b - \boldsymbol{R}(\hat{\boldsymbol{q}}^t_b)\right)\boldsymbol{r}^b_b\|_2. \end{aligned} \tag{27}$$

For position dead reckoning, only NLO A is to be considered. This is because of NLO B's innate dependency on position reference measurements. In a dead reckoning case, one would have to cut the feedback interconnection and use the same reference vector as for NLO A, effectively making the NLOs the same. A possibility to get the best of both worlds would be to create a switching mechanism for using NLO B's more accurate attitude estimates as we enter dead reckoning and switch over to using NLO A afterwards, but that is beyond the scope of this article.

For the dead reckoning test, an accelerometer bias average estimate based on the last minute of the $\hat{\boldsymbol{b}}^b_{\text{acc}}$ state is used. This is to account for any short term fluctuations of the accelerometer bias and GNSS imprecisions. The same could be achieved by tuning the matrices $\boldsymbol{Q}$ and $\boldsymbol{R}$ differently, at the expense of estimator convergence time. Fig. 8 displays an example of a dead reckoning run with ADIS16485. The position estimate starts drifting immediately after feedback is cut at $t = 15$ minutes. Fig. 9 shows the aggregated drift errors over 10 minutes, after PosRef injection is disabled, applying NLO A and Σ_3 for both the ADIS16485 and the STIM300 IMU. The statistical results based on the 60 dead reckoning runs are presented in Tab. XI.

C. Discussions

1) Heading dead reckoning: It is evident, with regards to Fig. 7, that the gyro bias estimates using the STIM300 is

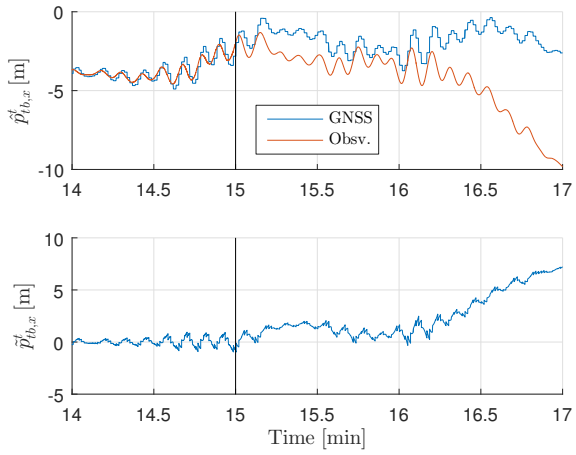

Fig. 8. Example of dead reckoning run with prior bias estimation, where feedback from GNSS is cut after 15 minutes (indicated by vertical line). North (or x) position on top, position difference between estimator and GNSS in bottom.

smoother and more in-run stable than those found using the ADIS16485, resulting in the performance difference seen in Fig. 6. This is in compliance with the sensor specifications presented in Tab. V. The asymptotic angular rate bias estimation performances seen in Fig. 7, is representative of what is seen from run to run.

2) Position dead reckoning: As seen from the "Standard" column of Tab. XI and Fig. 9, one of the main conclusions from the six times 60 dead reckoning runs performed over the data sets collected during DP is that using the STIM300 results in better performance than using the ADIS16485. Interestingly enough, for the unfiltered data of the same table the opposite conclusion is reached. According to specifications, the ADIS16485 has the better accelerometer, while the STIM300 contains a superior angular rate sensor. One could speculate that by removing the white noise of the accelerometer through filtering, the errors induced by angular rate sensors become more important. In any case, from looking at the results of Tab. XI and Fig. 10 with no accelerometer bias estimation, one can see that estimating the residual accelerometer biases as in (21) clearly has a positive effect on the dead reckoning results.

The results indicate a large spread of dead reckoning errors over 10 minutes, and this might be due to noise, mechanical disturbance such as vibration, or insufficient tuning of the observers. Time synchronization of signals is also an issue, as the GNSS and gyrocompass signals were acquired from a system separate from the IMUs' signal acquisition, with an unknown, albeit small, delay.

Considering the quality of the results obtained compared to the results in [39], using either of the two MEMS-based IMUs available in this work gave worse results than in [39] where an INS with a FOG gyro was applied. In the results presented in [39], a position accuracy during GNSS outage stayed within GNSS accuracy for a period exceeding two and a half minutes. The mean position drift after a 50 seconds GNSS outage was less than half a meter. These results are considerably better

TABLE XI
POSITION DEAD RECKONING ERROR STATISTICS

	Standard (Fig. 9)		No acc bias (Fig. 10)		No pre-filtering	
	ADIS16485	STIM300	ADIS16485	STIM300	ADIS16485	STIM300
Mean error [m] 1 min	4.3014	3.2885	4.6148	3.9820	4.7580	4.3560
Mean error [m] 5 min	35.125	25.762	54.037	56.256	38.588	44.631
Mean error [m] 10 min	102.12	83.927	211.89	218.51	112.07	139.51
Min error [m] after 10 min	11.639	3.0962	76.464	120.83	4.1972	26.919
Max error [m] after 10 min	264.03	231.74	359.18	362.18	244.97	350.30
RMSE [m] after 10 min	115.74	96.141	220.24	224.94	125.25	159.93

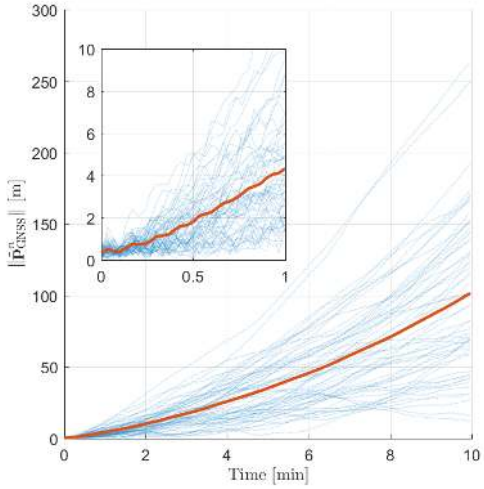

(a) Dead reckoning errors obtained with ADIS16485.

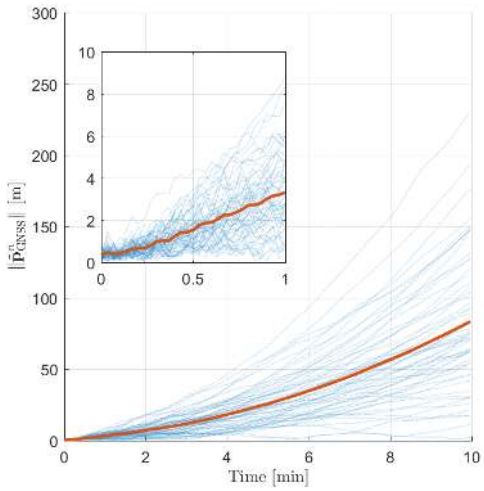

(b) Dead reckoning errors obtained with STIM300.

Fig. 9. Aggregated dead reckoning error over 60 runs using NLO A in minutes after position feedback is removed. Red indicates the mean error, blue lines are individual runs.

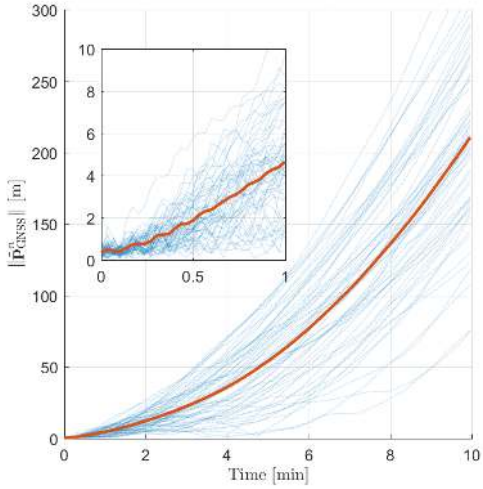

(a) Dead reckoning errors obtained with ADIS16485.

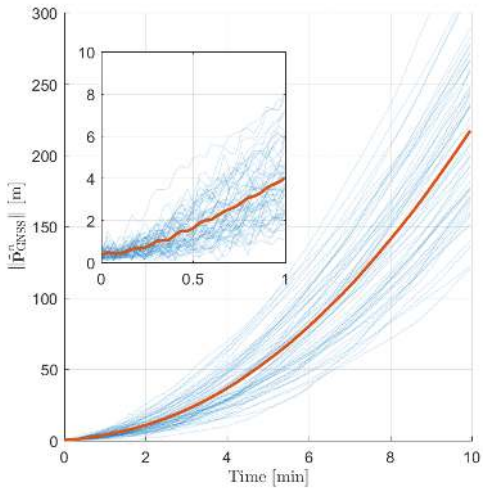

(b) Dead reckoning errors obtained with STIM300.

Fig. 10. Aggregated dead reckoning error over 60 runs using NLO A, and no bias estimation in Σ_3 in minutes after position feedback is removed. Red indicates the mean error, blue lines are individual runs.

than the approximately 3-5 meters error obtained after one minute dead reckoning for both MEMS IMUs. However, in [39] only 10 runs are presented, making a definite statistical comparison difficult due to the few dead reckoning trajectories presented. The FOG-based INS product in question is currently advertised to have a 20 m error with a 50 % circular error probability after five minutes of unaided navigation, whereas we obtain approximately 25 meters averaged error in the same time frame for STIM300.

As depicted in Fig. 9, a MEMS-based INS may provide

relatively stable position estimates (around four meters error) for half a minute, without PosRef injection. From a fault-tolerance perspective, the results obtained here indicate what kind of PosRef errors one might detect based on MEMS IMUs. For instance a PosRef drift of 10 centimeters per second results in a PosRef error of 3 meters after half a minute, which might be possible to detect with the results obtained, considering the average error is two meters with either of the two IMUs. Moreover, in the situation of PosRef failure during DP, if four meters is an acceptable error margin, 30 seconds is available to the DP operator to decide whether the operation should be aborted or not. This might be sufficient time for PosRef recovery e.g. if tracking is reestablished with one or more satellites, resulting in a complete GNSS solution.

The dead reckoning performance is not only dependent on the sensor biases, but also on the velocity-random walk and the sensed vibrations on the ship. Integrating these over time, results in a large error even when averaging them out using high-rate integration (1000 Hz). Low-pass filtering of the IMU signals may be beneficial, and compared to [36] where this was not done, some improvements are made in the drift-offs.

Regarding tuning, more emphasis on tuning for a dead reckoning application may accomplish better results. In this article, the tuning is geared towards attaining the smallest errors in attitude and heave compared to the onboard VRU. Also, time-synchronization errors between our IMUs and the onboard GNSS may result in small errors in velocity and specific force at the time of disabling GNSS injection, resulting in a steeper error slope than otherwise obtained if the position and inertial measurements were synchronized.

IX. Concluding Remarks

The article set out to explore the credibility of using MEMS IMUs for complementing existing systems on board dynamically positioned vessels. A successful verification of two nonlinear estimators for attitude/vertical reference was carried out, employing two different MEMS IMUs, namely the ADIS16485 and STIM300. The full-scale experimental data was collected on an offshore vessel operating outside the Norwegian coast. Comparing the observer output to industry standard VRUs and navigation software based on EKF showed that favorable performance could be achieved, and that for attitude estimation the method was more important than the IMU itself. The results also showed that estimating specific force in the navigation frame improves attitude estimates, in contrast to assuming that the vessel is not accelerating. Heave estimation was also compared, revealing more differences between the IMUs. Seemingly ADIS16485 had a better accelerometer than STIM300, which reflected upon the results.

Dead reckoning for heading and position using the IMUs was also considered, where the heading case revealed the great qualities of the STIM300's angular rate sensors. For dead reckoning in position, the IMUs yielded comparable results with the STIM300 coming out on top, probably because of the better angular rate sensor. The results showed that it would be plausible to detect certain drifts of the position reference system using MEMS IMUs.

All in all, the performance of the INS based on MEMS IMUs suggests that they would be a valued addition to a DP system, whether the goal is to reduce the number of other external sensors and systems, or simply complementing existing systems.

Acknowledgment

This work has been carried out at the Centre for Autonomous Marine Operations and Systems (NTNU–AMOS) and supported by the Research Council of Norway and Rolls–Royce Marine (now Kongsberg Maritime CM) through the Centres of Excellence funding scheme and the MAROFF programme, grant numbers, 223254 and 225259 respectively. The Research Council of Norway is acknowledged as the main sponsor of NTNU–AMOS.

The authors wish to thank colleagues at the mechanical and electronics workshop at the Department of Engineering Cybernetics for help during the development of the sensor payload and thank Rolls–Royce Marine (now Kongsberg Martime CM) and Farstad Shipping (now Solstad Offshore) for assistance in the process of installing the sensor payload on board the offshore vessel. The authors wish to thank Farstad Shipping for allowing us to install the equipment on board. The authors wish to thank Sensonor for providing an engineering sample of the STIM300 IMU.

References

[1] M. N. Armenise, C. Ciminelli, F. Dell'Olio, and V. M. N. Passaro, *Advances in Gyroscope Technologies*. Berlin Heidelberg: Springer-Verlag, 2010.

[2] A. J. Sørensen, "A survey of dynamic positioning control systems," *Annual Reviews in Control*, vol. 35, pp. 123—136, 2011.

[3] T. I. Fossen, *Handbook of Marine Craft Hydrodynamics and Motion Control*. John Wiley & Sons, Ltd., 2011.

[4] International Maritime Organization, "Guidelines for vessels with dynamic positioning systems," *MSC/Circ 645*, pp. 1–16, 1994.

[5] DNV GL, "Newbuildings special equipment and systems – additional class: Dynamic positioning systems," in *Rules for classification of ships*. DNV GL, 2014, Part 6 Chapter 7.

[6] H. Chen, T. Moan, and H. Verhoeven, "Effect of dGPS failures on dynamic positioning of mobile drilling units in the North Sea," *Accident Analysis and Prevention*, vol. 41, no. 6, pp. 1164–1171, 2009.

[7] T. H. Bryne, R. H. Rogne, T. I. Fossen, and T. A. Johansen, "Inertial sensors for risk-based redundancy in dynamic positioning," in *ASME 2017 36th International Conference on Ocean, Offshore and Arctic Engineering*. Trondheim: American Society of Mechanical Engineers, Jun. 2017, pp. V001T01A069–V001T01A069.

[8] M. J. Ingram, R. C. Tyce, and R. G. Allen, "Dynamic testing of state of the art vertical reference units." in *Proc. Oceans 96 MTS/IEEE*, 1996, pp. 1533–1538.

[9] P. D. Groves, *Principles of GNSS, Inertial, and Multisensor Integrated Navigation Systems*, 2nd ed. Norwood, MA: Artech House, 2013.

[10] D. H. Titterton and J. L. Weston, *Strapdown inertial navigation technology*, 2nd ed. Institution of Electrical Engineers and American Institute of Aeronautics and Astronautics, 2004.

[11] J. A. Farrell, *Aided Navigation: GPS with High Rate Sensors*. New York City, NY: McGraw-Hill, 2008.

[12] S. Salcudean, "A globally convergent angular velocity observer for rigid body motion," *IEEE Trans. Automat. Contr.*, vol. 36, no. 12, pp. 1493 – 1497, 1991.

[13] B. Vik and T. Fossen, "A nonlinear observer for GPS and INS integration," in *Proc. IEEE Conf. Dec. Cont*, vol. 3, Orlando, FL, December 2001, pp. 2956–61.

[14] R. Mahony, T. Hamel, and J. M. Pflimlin, "Nonlinear complementary filters on the special orthogonal group," *IEEE Transactions on Automatic Control*, vol. 53, no. 5, pp. 1203–2018, 2008.

[15] M.-D. Hua, "Attitude estimation for accelerated vehicles using GPS/INS measurements," *Control Engineering Practice*, vol. 18, no. 7, pp. 723–732, 2010.

[16] H. F. Grip, T. I. Fossen, T. A. Johansen, and A. Saberi, "Attitude estimation using biased gyro and vector measurements with time-varying reference vectors," *IEEE Transactions on Automatic Control*, vol. 57, no. 5, pp. 1332—1338, 2012.

[17] P. Batista, C. Silvestre, and P. Oliveira, "A GES attitude observer with single vector observations," *Automatica*, vol. 48, no. 2, pp. 388–39, 2012.

[18] ——, "Globally exponentially stable cascade observers for attitude estimation," *Control Engineering Practice*, vol. 20, no. 2, pp. 148–155, 2012.

[19] H. F. Grip, A. Saberi, and T. A. Johansen, "Observers for interconnected nonlinear and linear systems," *Automatica*, vol. 48, no. 7, pp. 1339–1346, 2012.

[20] H. F. Grip, T. I. Fossen, T. A. Johansen, and A. Saberi, "Nonlinear observer for GNSS-aided inertial navigation with quaternion-based attitude estimation," in *Proc. of the American Contr. Conf.*, Washington, DC, June 2013, pp. 272–279.

[21] ——, "Globally exponentially stable attitude and gyro bias estimation with application to GNSS/INS integration," *Automatica*, vol. 51, pp. 158—166, January 2015.

[22] T. H. Bryne, T. I. Fossen, and T. A. Johansen, "Nonlinear observer with time-varying gains for inertial navigation aided by satellite reference systems in dynamic positioning," in *Proc. of the IEEE Mediterranean Conference on Control and Automation*, Palermo, Italy, June 16–19 2014, pp. 1353–1360.

[23] ——, "A virtual vertical reference concept for GNSS/INS applications at the sea surface," in *Proc. of the 10th IFAC Conference on Manoeuvring and Control of Marine Craft*, Copenhagen, Denmark, Aug. 24–26 2015, pp. 127–133.

[24] T. H. Bryne, R. H. Rogne, T. I. Fossen, and T. A. Johansen, "A virtual vertical reference concept for integrated inertial navigation at the sea surface," *Control Engineering Practice*, n.d., submitted for publication.

[25] R. H. Rogne, T. A. Johansen, and T. I. Fossen, "On attitude observers and inertial navigation for reference system fault detection and isolation in dynamic positioning," in *Proc. European Control Conference (ECC)*, Linz, Austria, July 15–17 2015, pp. 3665–3672.

[26] M.-D. Hua, G. Ducard, T. Hamel, R. Mahony, and K. Rudin, "Implementation of a nonlinear attitude estimator for aerial robotic vehicles," *IEEE Transactions On Control System Technology*, vol. 22, no. 1, pp. 201–212, 2014.

[27] J.-M. Godhavn, "Adaptive tuning of heave filter in motion sensor," in *OCEANS '98 Conf. Proc.*, vol. 1, Nice, France, 28 Sept.–1 Oct. 1998, pp. 174–178.

[28] S. Küchler, J. K. Eberharter, K. Langer, K. Schneider, and O. Sawodny, "Heave motion estimation of a vessel using acceleration measurements," in *Proc. of the 18th IFAC World Congress*, MIlan, Italy, 2011, pp. 14 742–14 747.

[29] M. Richter, K. Schneider, D. Walser, and O. Sawodny, "Real-time heave motion estimation using adaptive filtering techniques," in *Proc. of the 19th IFAC World Congress*, Cape Town, South Africa, 2014, pp. 10 119–10 125.

[30] K. Vickery, "The development and use of an inertial navigation system as a DP position reference sensor (IPRS)," in *Proc. of the Dynamic Positioning Conference*, Houston, TX, Oct. 12–13 1999.

[31] M. Berntsen, "Hydroacoustic aided inertial navigation system – HAIN a new reference for DP," in *Proc. of the Dynamic Positioning Conference*, Houston, TX, Oct. 9–10 2007.

[32] M. Carter, "DP INS – a paradigm shift?" in *Proc. of the Dynamic Positioning Conference*, Houston, TX, Oct. 11–12 2011.

[33] R. H. Rogne, T. H. Bryne, T. I. Fossen, and T. A. Johansen, "Redundant mems-based inertial navigation using nonlinear observers," *Journal of Dynamic Systems, Measurement, and Control*, vol. 140, no. 7, p. 071001, 2018.

[34] R. I. Stephens, "Wind feedforward: blowing away the myths," in *Proc. of the Dynamic Positioning Conference*, Houston, TX, Oct. 11–12 2011.

[35] T. H. Bryne, R. H. Rogne, T. I. Fossen, and T. A. Johansen, "Attitude and heave estimation for ships using mems-based inertial measurements using MEMS-based inertial measurements," in *Proc. of the 10th IFAC Conference on Control Applications in Marine Systems*, Trondheim, Sep. 2016, pp. 568—575.

[36] R. H. Rogne, T. H. Bryne, T. I. Fossen, and T. A. Johansen, "MEMS-based inertial navigation on dynamically positioned ships: Dead reckoning," in *Proc. of the 10th IFAC Conference on Control Applications in Marine Systems*, Trondheim, Sept. 13–16 2016, pp. 139—146.

[37] R. Kalman and R. Bucy, "New results in linear filtering and prediction theory," *American Society of Mechanical Engineers – Transactions – Journal of Basic Engineering Series D*, vol. 83, no. 1, pp. 95–108, 1961.

[38] K. Gade, "Navlab, a generic simulation and post-processing tool for navigation," *European Journal of Navigation*, vol. 2, no. 4, pp. 51–59, 2004. [Online]. Available: http://www.navlab.net/Publications/

[39] Y. Paturel, "PHINS, an all-in-one sensor for DP applications," in *Proc. of the Dynamic Positioning Conference*, Houston, TX, Sept. 28–30 2004.